


FULL ARTICLE

Highly sensitive lipid detection and localization in atherosclerotic plaque with a dual-frequency intravascular photoacoustic/ultrasound catheter

Yingchun Cao¹ | Mouhamad Alloosh² | Michael Sturek² | Ji-Xin Cheng^{1,3} 

¹Department of Electrical and Computer Engineering, Boston University, Boston, Massachusetts

²Department of Anatomy, Cell Biology & Physiology, Indiana University School of Medicine, Indianapolis, Indiana

³Department of Biomedical Engineering, Boston University, Boston, Massachusetts

Correspondence

Ji-Xin Cheng, Department of Electrical and Computer Engineering, Boston University, 8 Saint Mary's Street, Boston, MA 02215.
Email: jxcheng@bu.edu

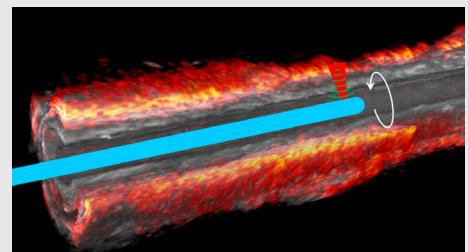
Michael Sturek, Department of Anatomy, Cell Biology & Physiology, Indiana University School of Medicine, 635 Barnhill Drive, Indianapolis, Indiana 46202.
Email: msturek@iupui.edu

Funding information

Center of Excellence in Cardiovascular Research Grant; Fortune-Fry Ultrasound Research Fund; Joshua Diabetes Research Fund; NIH, Grant/Award Number: R01 HL125385

Abstract

Intravascular photoacoustic/ultrasound (IVPA/US) is an emerging hybrid imaging modality that provides specific lipid detection and localization, while maintaining co-registered artery morphology, for diagnosis of vulnerable plaque in cardiovascular disease. However, current IVPA/US approaches based on a single-element transducer exhibit compromised performance for lipid detection due to the relatively low contrast of lipid absorption and conflicting detection bands for photoacoustic and ultrasound signals. Here, we present a dual-frequency IVPA/US catheter for highly sensitive detection and precision localization of lipids. The low-frequency transducer provides enhanced photoacoustic sensitivity, while the high-frequency transducer maintains state-of-the-art spatial resolution for ultrasound imaging. The boosted capability of IVPA/US imaging enables a multi-scale analysis of lipid distribution in swine with coronary atherosclerosis. The dual-frequency IVPA/US catheter has a diameter of 1 mm and flexibility to easily adapt to current catheterization procedures and is a significant step toward clinical diagnosis of vulnerable plaque.



KEYWORDS

atherosclerotic plaque, dual-frequency, intravascular photoacoustic, lipid core, Ossabaw miniature swine

1 | INTRODUCTION

Atherosclerosis is the major form of cardiovascular disease and the leading cause of morbidity and mortality throughout the world. The acute coronary syndrome is caused by a thrombus, 60%-70% of which originates from

plaque rupture in atherosclerotic lesions.^[1] This kind of vulnerable plaque is called thin cap fibroatheroma, which is characterized by a lipid-rich necrotic core covered by a thin fibrous cap (<65 μm), with numerous macrophages and inflammation.^[2] Rupture and thrombosis can occur in lesions that are not critical, flow-limiting to require

This is an open access article under the terms of the Creative Commons Attribution License, which permits use, distribution and reproduction in any medium, provided the original work is properly cited.

© 2020 The Authors. *Translational Biophotonics* published by WILEY-VCH Verlag GmbH & Co. KGaA, Weinheim

coronary interventions, such as angioplasty or stenting. Therefore, quantification of the lipid and depth in this vulnerable plaque could prompt coronary interventions to prevent the acute coronary syndrome. Currently, the most common approach used in clinical diagnosis of atherosclerosis is x-ray angiography.^[3] However, it only provides information on critical stenosis of the artery. Intravascular ultrasound is another commonly used method to identify the vulnerable plaque.^[4] Recently, acoustic radiation force-based intravascular ultrasound elastography with dual-frequency transducer was developed for the characterization of coronary plaque.^[5] However, these ultrasound-based modalities lack useful chemical information. Intravascular optical coherence tomography attracts special attention due to its exceptional spatial resolution to identify the thickness of the thin cap.^[6] However, the insufficient imaging depth (~1-2 mm) and the requirement of blood clearance or balloon occlusion limit its extensive application. Other recently developed intravascular imaging tools,^[7] such as near-infrared spectroscopy,^[8] near-infrared fluorescence,^[9] and fluorescence lifetime imaging^[10] can provide useful molecular information of the arterial wall. Nevertheless, they lack depth resolution to evaluate the entire arterial wall.

Intravascular photoacoustic/ultrasound (IVPA/US) imaging is a hybrid imaging modality that combines molecular information through photoacoustically induced ultrasound generation with artery morphology via conventional ultrasound.^[11] With nanosecond pulsed laser wavelength falling in the overtone absorption range of C-H bond at 1.2 or 1.7 μm , specific lipid distribution can be resolved from the arterial wall.^[12] Over the last decade, almost all the IVPA catheter designs are based on a single element transducer for both photoacoustic and ultrasound detection, through collinear^[12b, 13] or cross overlap^[11a, 14] between optical and ultrasound paths. However, due to relatively weak absorption of endogenous lipid at these wavelengths compared to other strong absorbers such as blood at visible range^[15] and contrast agents in the infrared range,^[16] the contrast of photoacoustic signal based on this configuration is not sufficient to accurately detect arterial lipid content. This insufficient sensitivity is more evident under in vivo conditions due to attenuation in blood and sheath material.^[17] Thus, improving the sensitivity for lipid detection without sacrificing the quality of ultrasound is important for the translation of IVPA technology.

By investigating the spectral performance of photoacoustic signals of lipid, it was found that the central frequency of detected lipid signals falls in a much lower frequency range (usually <10 MHz), instead of near that of the ultrasound transducer (~40 MHz) used in IVPA catheters.^[18] This indicated that photoacoustic detection in reported IVPA catheter designs can be further optimized

by using a lower frequency transducer. However, to ensure suitable IVUS resolution for precision localization, a higher frequency transducer for ultrasound imaging is also necessary. Based on these requirements, we developed a dual-frequency IVPA/US catheter, with its low-frequency transducer assigned for photoacoustic detection, while a high-frequency transducer is used for the conventional ultrasound to provide high-resolution of morphology. The imaging catheter was evaluated for ex vivo imaging of an atherosclerotic pig coronary artery to assess its potential for in vivo preclinical and clinical applications.

2 | MATERIALS AND METHODS

2.1 | Configuration of imaging system

The schematic of our dual-frequency IVPA/US imaging system is depicted in Figure 1. Nanosecond optical pulses at 1725 nm from an optical parametric oscillator light source with a repetition rate of 500 Hz was employed for photoacoustic excitation.^[12c] The laser pulses were coupled to the imaging catheter through an optical fiber and a self-built fiber-optic rotary joint. Co-registered photoacoustic and ultrasound images were obtained separately at the tip of a dual-frequency catheter through a motorized helical scanning of the catheter. The optical pulse energy output from the catheter tip is kept at 100 μJ , or ~0.3 J/cm^2 , which is much less than the ANSI laser safety standard of 1.0 J/cm^2 at this wavelength. A dual-channel slip ring (JINPAT Electronics, China) was used to transmit the electric signal to/from the transducers. A pulser/receiver (5073PR, Olympus, Inc.) together with a delay generator (9512, Quantum Composers, Inc.) was used to send/detect ultrasound signals. The trigger of the laser pulse was obtained via a fast photodetector (DET10A, Thorlabs, Inc.) and used as a reference for ultrasound emission and data acquisition. Real-time data acquisition and image processing were implemented through a high-speed DAQ card (ATS9462 PCI express digitizer, 180 MS/s, 16 bit, AlazarTech, Canada) and a self-programmed LabVIEW (National Instruments Corp.) interface.

2.2 | Dual-frequency IVPA/US catheter

To optimize the photoacoustic detection while maintaining a suitable ultrasound spatial resolution for precision localization, we proposed a dual-frequency IVPA/US catheter design as in Figure 2A. Laser pulses were delivered within a multimode fiber (FG200LEA, 200 μm core, 0.22 NA, Thorlabs, Inc.). Side firing was implemented by total internal reflection at an uncoated micro-prism (0.3 mm leg,

FIGURE 1 Schematic of dual-frequency IVPA/US imaging. FORJ: fiber-optic rotary joint. IVPA/US, intravascular photoacoustic/ultrasound

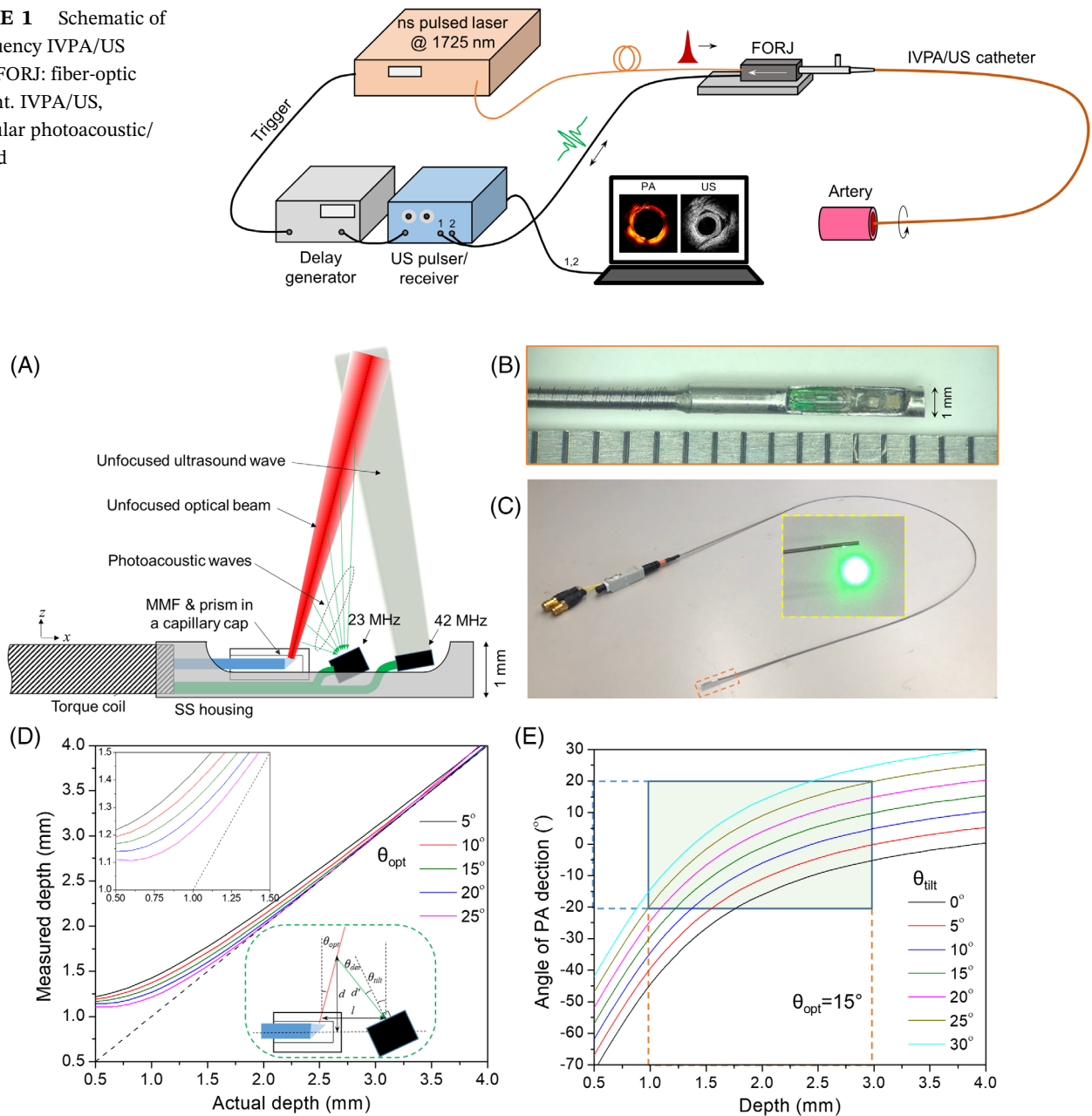


FIGURE 2 Dual-frequency IVPA/US catheter design and optimization. A, Design of a dual-frequency IVPA/US catheter; B, photograph of fabricated catheter tip; C, entire catheter; D, optimization of optical firing angle from the catheter tip, with the upper inset showing a zoom-in at small depth, and the lower inset depicting the geometrical relationship between fiber tip and 23 MHz transducer; E, optimization of tilted angle of 23 MHz transducer with light firing angle of 15° to the vertical direction, the green area showing the effective detection region and acceptance angle of the transducer. IVPA/US, intravascular photoacoustic/ultrasound

Precision Optics Corp.) attached to the fiber end and enclosed in a glass capillary. This configuration can avoid the issue of low optical damage threshold in commonly used metal-coated prisms, while preventing the optical beam distortion induced by lensing effect in angle-polished fiber end reflection (see inset in Figure 2C). Considering the catheter dimension limitations (usually ~ 1 mm in diameter), a low-frequency transducer (23 MHz, 60% bandwidth, Blatek, Inc.) was placed next to the fiber tip for

photoacoustic signal detection, while another high-frequency transducer (42 MHz, 50% bandwidth, Blatek, Inc.) was placed further for conventional ultrasound pulsing/receiving with satisfactory axial resolution. The optical components and transducers were well-aligned and enclosed in stainless steel housing. A torque coil (Asahi Intecc, Inc.) was used to transmit the torque to the catheter tip and provide the necessary robustness and flexibility of the catheter.

The angle-dependent sensitivity of the transducer and noncollinear overlap between optics and acoustics requires a specific combination of light firing angle and transducer tilted angle in the catheter. Considering a separation distance of 1 mm between 23 MHz transducer and emission point of optical beam (l as shown in the inset of Figure 2D), the measured depth (d') at each corresponding actual depth (d) was calculated for different light emission angles as shown in Figure 2D. To ensure a resolvable depth close to the catheter and efficient overlap between optics and ultrasound, we selected an optical firing angle of 15° regard to the vertical direction. This was realized by introducing a polished angle of 7.5° at the fiber tip (Figure 2D). Based on this illumination angle, the photoacoustic detection angle to the normal direction of the low-transducer surface (θ_{det}) was calculated for different transducer tilted angles (θ_{tilt}) as shown in Figure 2E. Usually, the acceptance angle of a \sim MHz PZT transducer falls within $\pm 20^\circ$ considering the enlarged optical beam size in tissue.^[19] Therefore, within an effective depth range of 1 to 3 mm, an optimized titled angle of 25° was selected to allow a sensitive photoacoustic detection within this depth range (Figure 2E). The high-frequency transducer was tilted by 10° as usual to avoid ultrasound artifact from the sheath. With these optimized

angles, we fabricated a dual-frequency IVPA/US catheter with an outer diameter of 1 mm as shown in Figure 2B,C. Please be noted that due to the separation distance between the photoacoustic excitation and high-frequency ultrasound detection along the catheter, an approximate offset of 1.2 mm between photoacoustic and ultrasound images was compensated to ensure coregistration between these two imaging modalities.

2.3 | Fiber-optic rotary joint and time sequence design

A section of the same type of optical fiber was butt connected to the coupling fiber and light delivering fiber in the catheter at both ends. Precision mechanics were designed and machined to provide a highly efficient light coupling during rotation and stable driving of the imaging catheter (Figure 3A). A laser beam at target wavelength was launched into the rotary joint, and transmitted light intensity from the other end was monitored during continuous rotary rotation and is displayed in Figure 3B. A power variation of 3.48% and insertion loss of <2 dB was observed for the rotational light coupling. A dual channel slip ring was used to transmit the

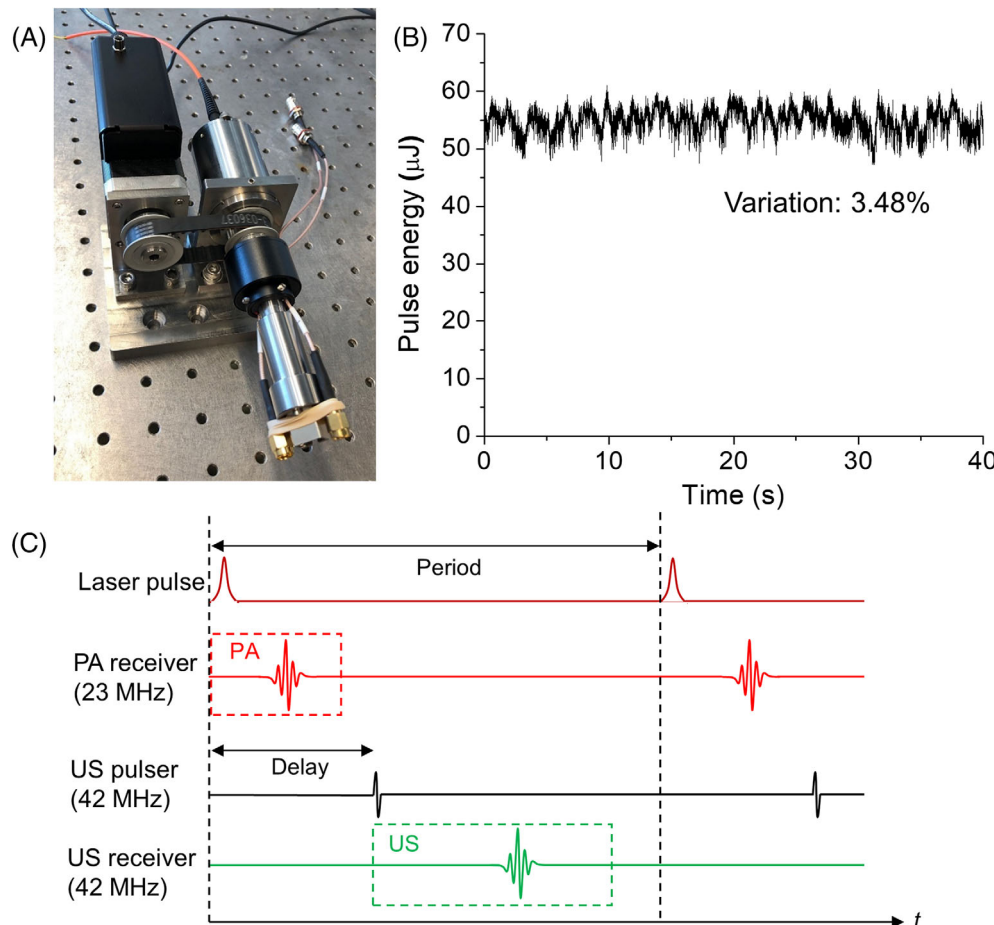


FIGURE 3 Optical and electrical coupling, and time sequence design. A, Photograph of a hybrid fiber-optic and electrical rotary joint; B, coupled optical pulse energy monitoring during continuous 10 revolutions; C, strategy of time sequence design of the two transducer channels

signals from both transducers. A stepper motor and linear stage combination were used to control the helical scanning of the catheter.

In each optical pulse cycle, the photoacoustic signal from the low-frequency transducer was acquired to form a photoacoustic image of lipid. A delayed ultrasound signal was fired to the arterial wall and its echo was collected by a high-frequency transducer to generate the ultrasound image as shown in Figure 3C.

2.4 | Preparation of pig coronary artery and implementation of ex vivo IVPA/US imaging

The right coronary artery of an Ossabaw miniature swine was harvested for validating our catheter for imaging of atherosclerotic plaque. The swine were fed a hypercaloric, atherogenic diet for 23 months to mimic the natural development of human coronary artery

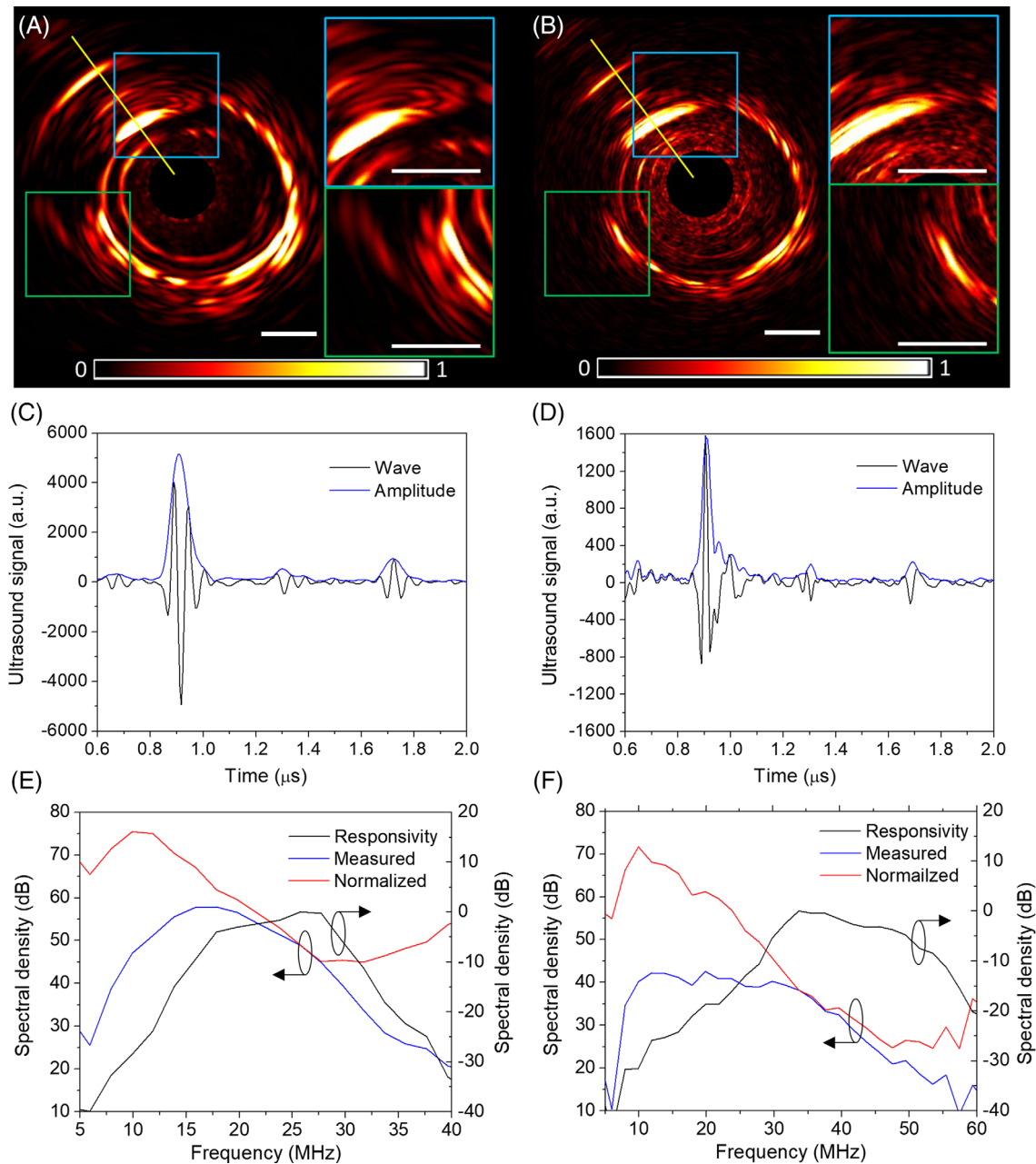


FIGURE 4 Comparison between 23 and 42 MHz transducers for detection of lipid deposit in artery using a collinear catheter design. A, B, Normalized photoacoustic images with zoom-in display of selected regions; C, D, A-line signal and amplitude along the yellow line in, A, B; E, F, frequency response of photoacoustic signals in, C, D. The black lines in, E, F, are responsivity of transducers characterized by measuring the ultrasound echo from a rigid surface, the blue lines are frequency domain expression of measured signal, while the red lines are their normalized result to the responsivity. A, C, E, correspond to 23 MHz catheter, and, B, D, F, are for 42 MHz transducer

disease.^[20] The fresh artery was excised and fixed in 10% neutral buffered formalin for further use.

To perform ex vivo imaging, the fixed artery was placed in 1x phosphate-buffered saline solution, and then our dual-frequency catheter was inserted into the lumen of the artery and helical scanning was performed to obtain 3D images of the entire artery. To avoid artifact due to water absorption and reduce light intensity loss when passing the lumen, the lumen of the artery was flushed with D₂O during imaging due to its much smaller absorption strength at 1725 nm. A rotational speed of 1 revolution per second and pullback speed of 0.1 mm per second was used for imaging. Images acquired at 1 frame per second were displayed and saved in real time via a LabVIEW interface.

2.5 | Histopathology validation

The fixed artery sample was cut into 2-mm-long segments. For each segment, representative slices from the paraffin-embedded artery was stained with hematoxylin and eosin to show the morphology of the artery.

Histology slides at each corresponding position were compared with IVPA/US imaging results to validate the performance of our imaging catheter.

3 | RESULTS

3.1 | Comparison of lipid detection at different frequencies

To determine the effective frequency range for photoacoustic detection, we designed a comparison experiment by measuring a lipid sample from an artery. Two collinear IVPA catheters^[13] with single element transducer design were employed for imaging, one with a 23 MHz transducer and the other with a 42 MHz transducer. The two catheters were used for IVPA imaging of a pig artery at the same location under the same conditions. The reconstructed photoacoustic images from these two catheters are shown in Figure 4A and B with normalization to their peak intensities, respectively. Two corresponding regions were highlighted to better indicate the difference

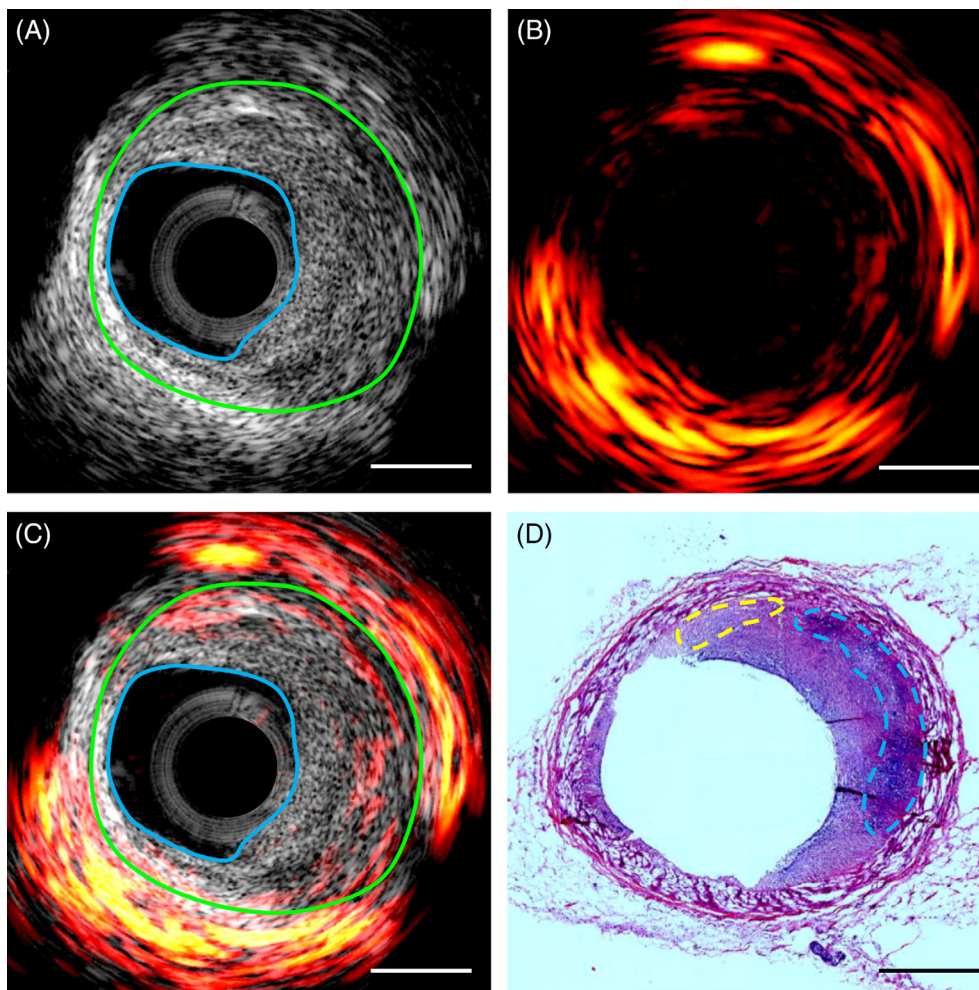


FIGURE 5 Representative imaging results and histology validation. A, Ultrasound, B, photoacoustic, C, their overlaid resulting image at a representative cross-sectional location of the pig artery. The region between the blue line and green line indicates a thickened intima, that is, atherosclerotic plaque; D, hematoxylin and eosin histology result at the same artery location. The blue line indicates lipid core, while the yellow lines denotes its early-stage lipid deposits. Scale bar of 1 mm applies to all the panels

between these two images. As can be seen, the two images have a very similar pattern, except that the 23 MHz image shows much stronger photoacoustic intensity and more details at different depth due to its high sensitivity. A representative A-line signal and its amplitude along the same direction indicated by the yellow line was plotted in Figure 4C,D for both catheters. For the corresponding lipid region, the averaged peak photoacoustic amplitude for 23 MHz catheter is found to be ~ 3.3 times larger than that by the 42 MHz catheter. The background noise level far away from the absorbers was measured to be comparable for these two catheters (11.4 for 23 MHz vs 10.3 for 42 MHz). Therefore, the 23 MHz catheter exhibit a three times stronger single-to-noise ratio than that of 42 MHz catheter at the same condition, indicating the 23 MHz transducer is not only sensitive for large lipid core detection but also capable for deep lipid components mapping. We further investigated the frequency domain performance of these two transducers. Photoacoustic signals in Figure 4C,D were expressed in the frequency domain as shown in Figure 4E,F in blue lines. After normalization to the responsivity of the transducers (black lines), we found in both cases the detected

photoacoustic signals from lipid fall in a spectral range centered at ~ 10 MHz, which agrees with our previously reported results.^[18a] This suggests a lower frequency (here 23 MHz) transducer is more suitable for photoacoustic detection of lipid in the arterial wall. This also forms the foundation of our dual-frequency IVPA/US catheter design.

3.2 | Imaging of pig coronary artery *ex vivo*

Our dual-frequency IVPA/US catheter was evaluated by intravascular imaging of a pig coronary artery *ex vivo*. Representative ultrasound, photoacoustic, and their overlaid images at a specific position is displayed in Figure 5A-C. For validation purposes, histology slides with hematoxylin and eosin staining at the corresponding position are provided in Figure 5D. Excessive plaque burden can be identified from the ultrasound image (highlighted region between blue and green lines in Figure 5C) and corroborated by histology (Figure 5D). The photoacoustic image indicates both abundant

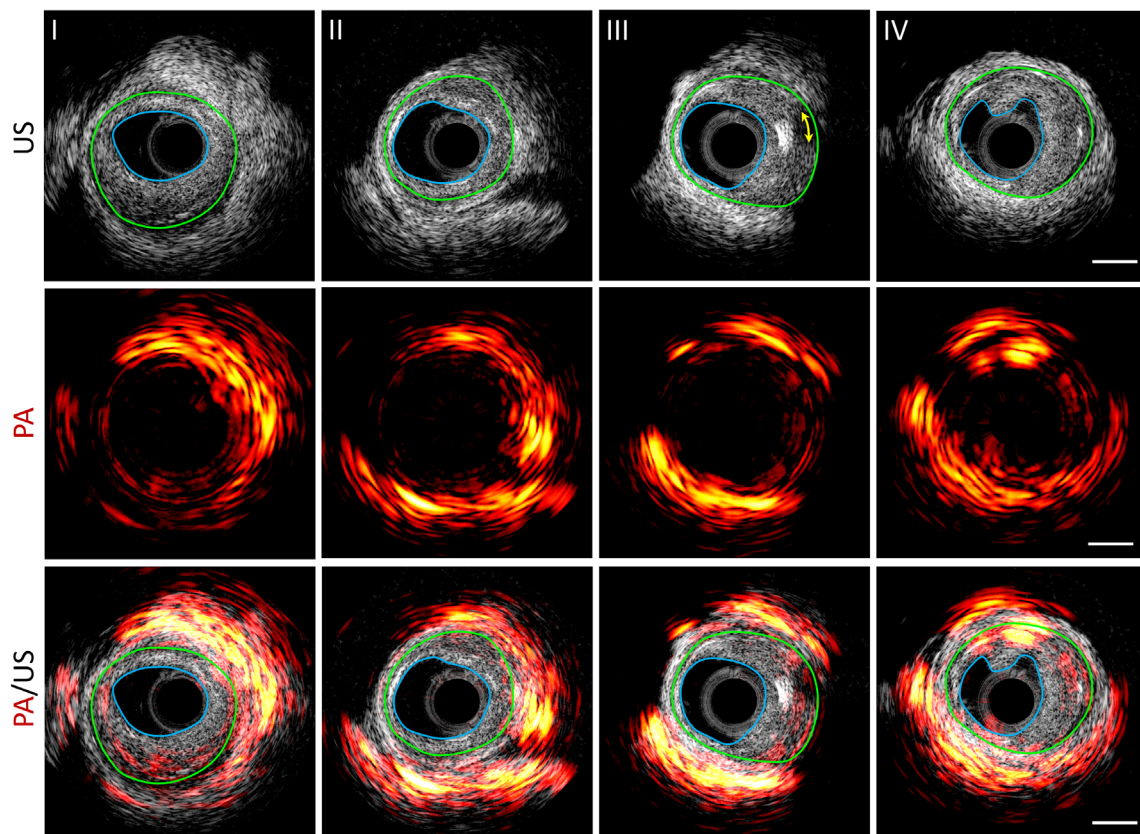


FIGURE 6 Photoacoustic (PA), ultrasound (US), and their overlaid images at representative positions along a pig coronary artery. Scale bar of 1 mm (right column) applies to all the panels. The blue line denotes the boundary of lumen and the green line indicates the boundary of the neointima layer (boundary of initial lumen). The yellow arrowed line in III indicates the acoustic shadowing behind an echogenic calcium nodule

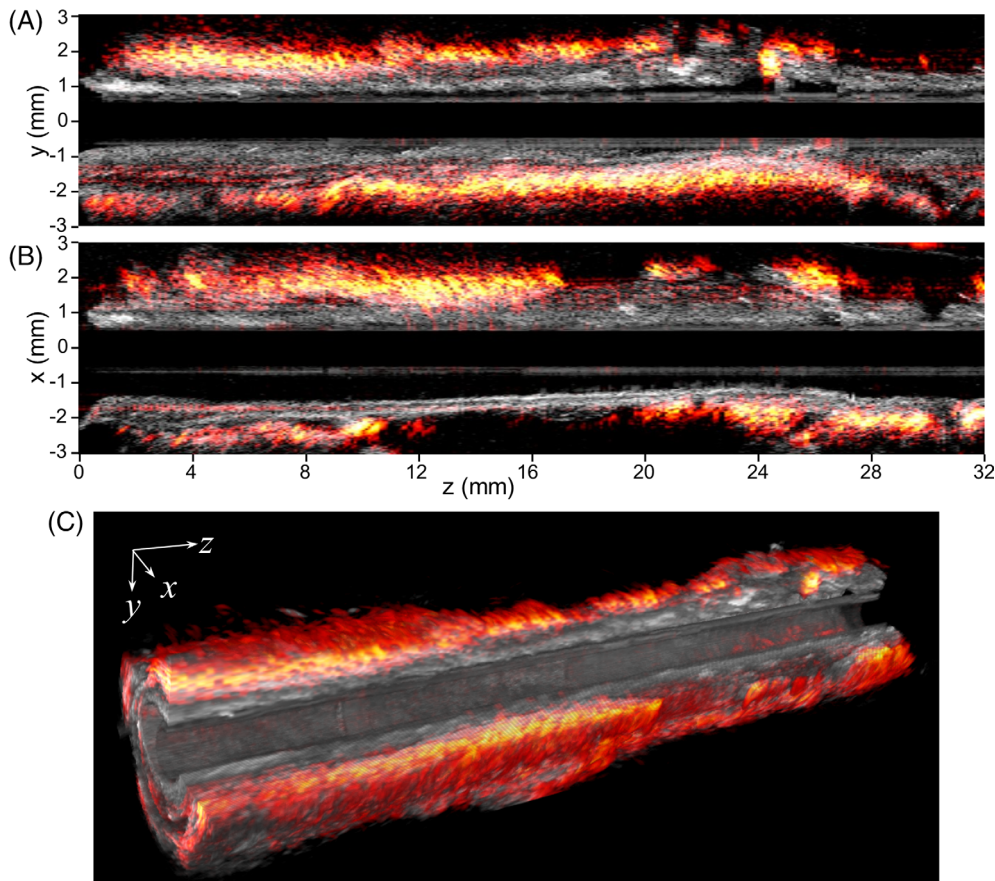


FIGURE 7 2D and 3D overlaid photoacoustic/ultrasound images over the pullback of the IVPA/US transducer through 32 mm length of artery. A, B, Overlaid photoacoustic/ultrasound images in yz and xz planes, respectively, C, 3D photoacoustic/ultrasound images of the artery with a 24 mm section length and a quarter cutaway for better visualization. IVPA/US, intravascular photoacoustic/ultrasound

perivascular fat and lipid deposits in the plaque region in Figure 5C. This was confirmed by the morphology of perivascular adipose tissue and lipid cores in hematoxylin and eosin stain. The blue line shows lipid-rich necrotic core, while the yellow line suggests early-stage lipid deposits. This agreement of lipid mapping throughout the depth between imaging result and histology indicates a unique strength of IVPA/US in detecting both lipid-rich plaque and perivascular fat tissue. We showed previously that we were able to quantify and localize the lipid in these lipid core lesions using IVPA/US, but not with near-infrared spectroscopy coupled with IVUS.^[21]

More imaging results at different locations of the artery were displayed in Figure 6 to show different plaque types of the pig artery. It reveals that plaques with intima thickening (region between blue and green profiles) from moderate level (II) to advanced levels (I, III, IV) of plaque burden were observed in this piece of artery, and mixed fibrous/calcified plaque (III) was also identified from the shadowed region denoted by a yellow double arrow line in the ultrasound image. In photoacoustic images, besides the abundant lipid detected in the perivascular adipose tissue as expected, lipid area in the plaque region (between blue and green curves) shows a positive correlation with the thickness of the plaque,

indicating its potential to evaluate the plaque vulnerability. The photoacoustic signal in the lumen of Figure 6 (IV) is an artifact due to the contamination of catheter tip.

The cutaway photoacoustic/ultrasound images in two perpendicular directions along the axis of the artery are displayed in Figure 7A,B to show the lipid distribution and artery morphology variation in a larger view. The co-registration of photoacoustic and ultrasound is further confirmed from these views. Overall, the lipid is found to be mainly from the perivascular fat tissue, with minor distribution in the arterial wall plaque region, agreeing with previous cross-sectional images. Figure 7C gives a more comprehensive view of lipid distribution in a 3D manner. It reveals that perivascular fat does not uniformly cover the arterial wall; instead, it varies dramatically.^[22]

4 | DISCUSSION

Early-stage plaque identification and staging under in vivo conditions is a long-standing challenge, but of high importance for the diagnosis of lipid-laden, vulnerable plaque development. Dual-modal IVPA/US provides

unique advantages in artery morphology measurement and lipid mapping with depth resolution. However, the intrinsic limitations of currently used transducers in IVPA imaging prevent the sensitive photoacoustic signal collection and high-resolution ultrasound imaging at the same time due to the narrow bandwidth of piezoelectric transducers. This limitation has greatly hindered progress toward clinical translation of IVPA imaging. Our dual-frequency IVPA catheter makes a major step in overcoming this limitation by using two transducers at different frequencies for separate photoacoustic and ultrasound detection. We showed much enhanced photoacoustic sensitivity and high-quality ultrasound imaging is enabled by this catheter design. This improvement in photoacoustic sensitivity could make a big impact during in vivo imaging, where photoacoustic contrast from plaque is hindered by blood scattering and water absorption. Another major advance of our dual-frequency catheter is the boosted photoacoustic signal from perivascular adipose tissue, which could enable the study of the atherogenic effect of perivascular lipid in vivo.^[22]

Considering the independent detection of photoacoustic and ultrasound, the axial resolution of ultrasound imaging can be further improved by using an ultra-high frequency transducer to be comparable with that of optical coherence tomography.^[23] Therefore, a fully upgraded dual-frequency IVPA/US catheter can potentially be able to detect the lipid core and thin fibrous cap at the same time without blood flushing or occlusion. This would enable IVPA/US to differentiate vulnerable plaque from other types of plaques because the volume of the lipid core and the thickness of the fibrous cap are both determinants of plaque vulnerability.^[1-3]

The dual-frequency catheter design presented in this work is not the final form of an IVPA catheter. Further, engineering strategies can be adapted to optimize its design, such as using a shorter metallic housing to reduce the length of the rigid part, applying dielectric coated mirror on the fiber end for light redirection to reduce the catheter diameter, and so on. Although the dual transducers increase the complexity and expense of the catheter, which could affect its clinical translation, it provides a possibility and future direction of the IVPA/US catheter development, that is, a single element transducer with extremely broadband coverage in the low frequency for photoacoustic detection and high frequency for high spatial resolution ultrasound mapping.

5 | CONCLUSION

IVPA imaging provides both artery morphology measurement and depth-resolved lipid mapping in vulnerable

plaque identification. A dual-frequency IVPA/US catheter is developed to address the long-standing limitations in single-element-transducer catheter design. With a diameter of 1 mm, the new catheter exhibits enhanced photoacoustic sensitivity, while maintaining state-of-the-art ultrasound characterization of arterial morphology. Imaging of an Ossabaw miniature swine coronary artery that superbly mimics human coronary atherosclerosis demonstrated that this catheter provides superior lipid detection and localization in both perivascular tissue and plaque region. These data promise a great opportunity for IVPA/US imaging technology in accurate diagnosis of vulnerable plaque in the clinic.

ACKNOWLEDGMENTS

We would like to acknowledge the financial support from NIH R01 HL125385, Center of Excellence in Cardiovascular Research Grant, Fortune-Fry Ultrasound Research Fund, and Joshua Diabetes Research Fund. We thank Ms. Cheryl Spencer from Boston Medical Center for providing service of artery sample sectioning and staining.

CONFLICT OF INTEREST

The authors declare no potential conflict of interests.

AUTHOR CONTRIBUTIONS

Yingchun Cao and Ji-Xin Cheng conceived the idea. Yingchun Cao designed and built the imaging catheter, setup the imaging system, performed experiment, and data processing. Mouhamad Alloosh and Michael Sturek provided and prepared the pig coronary artery samples. Michael Sturek provided important input in atherosclerosis and artery pathology. All authors contributed to the manuscript writing.

ORCID

Ji-Xin Cheng  <https://orcid.org/0000-0002-5607-6683>

REFERENCES

- [1] E. Falk, K. Shah Prediman, V. Fuster, *Circulation* **1995**, 92 (3), 657.
- [2] a R. Virmani, A. P. Burke, F. D. Kolodgie, A. Farb, *J. Interv. Cardiology* **2003**, 16(3), 267. b R. Virmani, A. P. Burke, A. Farb, F. D. Kolodgie, *J. Am. Coll. Cardiol.* **2006**, 47 (8), C13.
- [3] A. Wahle, J. J. Lopez, M. E. Olszewski, S. C. Vigmostad, K. B. Chandran, J. D. Rossen, M. Sonka, *Med. Image Anal.* **2006**, 10(4), 615.
- [4] J. M. Tarkin, M. R. Dweck, N. R. Evans, R. A. P. Takx, A. J. Brown, A. Tawakol, Z. A. Fayad, J. H. F. Rudd, *Circ. Res.* **2016**, 118(4), 750.
- [5] a Z. Wang, X. Jiang, T. J. Czernuszewicz, C. M. Gallippi, **2015** IEEE International Ultrasonics Symposium (IUS), Taipei, 2015, 1. <https://doi.org/10.1109/ULTSYM.2015.0119>. b C.-

- C. Shih, P.-Y. Chen, T. Ma, Q. Zhou, K. K. Shung, C.-C. Huang, R. Soc, *Open Sci.* **2018**, 5(4), 180138.
- [6] G. J. Tearney, E. Regar, T. Akasaka, T. Adriaenssens, P. Barlis, H. G. Bezerra, B. Bouma, N. Bruining, J. M. Cho, S. Chowdhary, M. A. Costa, R. de Silva, J. Dijkstra, C. Di Mario, D. Dudek, E. Falk, M. D. Feldman, P. Fitzgerald, H. M. Garcia-Garcia, N. Gonzalo, J. F. Granada, G. Guagliumi, N. R. Holm, Y. Honda, F. Ikeno, M. Kawasaki, J. Kochman, L. Koltowski, T. Kubo, T. Kume, H. Kyono, C. C. Lam, G. Lamouche, D. P. Lee, M. B. Leon, A. Maehara, O. Manfrini, G. S. Mintz, K. Mizuno, M. A. Morel, S. Nadkarni, H. Okura, H. Otake, A. Pietrasik, F. Prati, L. Raber, M. D. Radu, J. Rieber, M. Riga, A. Rollins, M. Rosenberg, V. Sirbu, P. W. Serruys, K. Shimada, T. Shinke, J. Shite, E. Siegel, S. Sonoda, M. Suter, S. Takarada, A. Tanaka, M. Terashima, T. Thim, S. Uemura, G. J. Ughi, H. M. van Beusekom, A. F. van der Steen, G. A. van Es, G. van Soest, R. Virmani, S. Waxman, N. J. Weissman, G. Weisz, T. International Working Group for Intravascular Optical Coherence, *J. Am. Coll. Cardiol.* **2012**, 59(12), 1058.
- [7] C. V. Bourantas, F. A. Jaffer, F. J. Gijsen, G. van Soest, S. P. Madden, B. K. Courtney, A. M. Fard, E. Tenekecioglu, Y. Zeng, A. F. van der Steen, S. Emelianov, J. Muller, P. H. Stone, L. Marcu, G. J. Tearney, P. W. Serruys, *Eur. Heart J.* **2016**, 38(6), 400.
- [8] C. M. Gardner, H. W. Tan, E. L. Hull, J. B. Lisauskas, S. T. Sum, T. M. Meese, C. S. Jiang, S. P. Madden, J. D. Caplan, A. P. Burke, R. Virmani, J. Goldstein, J. E. Muller, *Imaging* **2008**, 1(5), 638.
- [9] H. Yoo, J. W. Kim, M. Shishkov, E. Namati, T. Morse, R. Shubochkin, J. R. McCarthy, V. Ntziachristos, B. E. Bouma, F. A. Jaffer, G. J. Tearney, *Nat. Med.* **2011**, 17(12), 1680.
- [10] L. Marcu, J. A. Jo, Q. Fang, T. Papaioannou, T. Reil, J.-H. Qiao, J. D. Baker, J. A. Freischlag, M. C. Fishbein, *Atherosclerosis* **2009**, 204(1), 156.
- [11] a K. Jansen, A. F. W. van der Steen, H. M. M. van Beusekom, J. W. Oosterhuis, G. van Soest, *Opt. Lett.* **2011**, 36(5), 597. b H. W. Wang, N. Chai, P. Wang, S. Hu, W. Dou, D. Umulis, L. V. Wang, M. Sturek, R. Lucht, J. X. Cheng, *Phys. Rev. Lett.* **2011**, 106(23), 238106.
- [12] a K. Jansen, A. F. W. van der Steen, M. Wu, H. M. M. van Beusekom, G. Springeling, X. Li, Q. F. Zhou, K. K. Shung, D. P. V. de Kleijn, G. van Soest, *J. Biomed. Opt.* **2014**, 19(2), 026006. b P. Wang, T. Ma, M. N. Slipchenko, S. Liang, J. Hui, K. K. Shung, S. Roy, M. Sturek, Q. Zhou, Z. Chen, J. X. Cheng, *Sci. Rep.* **2014**, 4, 6889. c J. Hui, Q. Yu, T. Ma, P. Wang, Y. Cao, R. S. Bruning, Y. Qu, Z. Chen, Q. Zhou, M. Sturek, J.-X. Cheng, W. Chen, *Biomed. Opt. Express* **2015**, 6(11), 4557. d Z. Piao, T. Ma, J. Li, M. T. Wiedmann, S. Huang, M. Yu, K. Kirk Shung, Q. Zhou, C.-S. Kim, Z. Chen, *Appl. Phys. Lett.* **2015**, 107(8), 083701.
- [13] Y. Cao, J. Hui, A. Kole, P. Wang, Q. Yu, W. Chen, M. Sturek, J.-X. Cheng, *Sci. Rep.* **2016**, 6, 25236.
- [14] a A. B. Karpouk, B. Wang, S. Y. Emelianov, *Rev. Sci. Instrum.* **2010**, 81(1), 014901. b Y. Cao, A. Kole, J. Hui, Y. Zhang, J. Mai, M. Alloosh, M. Sturek, J. X. Cheng, *Sci. Rep.* **2018**, 8(1), 2400.
- [15] J. Hui, R. Li, E. H. Phillips, C. J. Goergen, M. Sturek, J. X. Cheng, *Photo-Dermatology* **2016**, 4(1), 11.
- [16] J. Wu, L. You, L. Lan, H. J. Lee, S. T. Chaudhry, R. Li, J. X. Cheng, J. Mei, *Adv. Mater.* **2017**, 29(41), 1703403.
- [17] a J. Hui, Y. Cao, Y. Zhang, A. Kole, P. Wang, G. Yu, G. Eakins, M. Sturek, W. Chen, J.-X. Cheng, *Sci. Rep.* **2017**, 7, 1417; b M. Wu, G. Springeling, M. Lovrak, F. Mastik, S. Iskander-Rizk, T. Wang, H. M. M. van Beusekom, A. F. W. van der Steen, G. Van Soest, *Biomed. Opt. Express* **2017**, 8(2), 943.
- [18] a Y. Cao, A. Kole, L. Lan, P. Wang, J. Hui, M. Sturek, J.-X. Cheng, *Photo-Dermatology* **2017**, 7, 12. b V. Daeichin, M. Wu, N. De Jong, A. F. W. van der Steen, G. van Soest, *Ultrasound Med. Biol.* **2016**, 42(8), 2017.
- [19] J. A. Guggenheim, E. Z. Zhang, P. C. Beard, *Ultrason. Ferroelectr. Freq. Control* **2017**, 64(12), 1857.
- [20] a Z. P. Neeb, J. M. Edwards, M. Alloosh, X. Long, E. A. Mokolke, M. Sturek, *Comp. Med.* **2010**, 60(4), 300; b M. L. McKenney-Drake, S. D. Rodenbeck, M. K. Owen, K. A. Schultz, M. Alloosh, J. D. Tune, M. Sturek, *Atherosclerosis* **2016**, 249, 1.
- [21] A. Kole, Y. Cao, J. Hui, I. A. Bolad, M. Alloosh, J.-X. Cheng, M. Sturek, *J. Cardiovasc. Transl. Res.* **2019**, 12(3), 211.
- [22] M. L. McKenney-Drake, S. D. Rodenbeck, R. S. Bruning, A. Kole, K. W. Yancey, M. Alloosh, H. S. Sacks, M. Sturek, *Ann. Thorac. Surg.* **2017**, 103(5), 1622.
- [23] T. Ma, M. Yu, J. Li, C. E. Munding, Z. Chen, C. Fei, K. K. Shung, Q. Zhou, *Ultrason. Ferroelectr. Freq. Control* **2015**, 62(1), 97.

How to cite this article: Cao Y, Alloosh M, Sturek M, Cheng J-X. Highly sensitive lipid detection and localization in atherosclerotic plaque with a dual-frequency intravascular photoacoustic/ultrasound catheter. *Translational Biophotonics*. 2020;e202000004. <https://doi.org/10.1002/tbio.202000004>